Front. Phys. 13(5), 130507 (2018)
https://doi.org/10.1007/s11467-018-0798-7

RESEARCH ARTICLE

Machine learning of frustrated classical spin models (II): Kernel principal component analysis

Ce Wang[1], **Hui Zhai**[1,2,†]

[1] *Institute for Advanced Study, Tsinghua University, Beijing 100084, China*
[2] *Collaborative Innovation Center of Quantum Matter, Beijing 100084, China*
Corresponding author. E-mail: [†]*huizhai.physics@gmail.com*
Received May 7, 2018; accepted May 21, 2018

In this work, we apply a principal component analysis (PCA) method with a kernel trick to study the classification of phases and phase transitions in classical XY models of frustrated lattices. Compared to our previous work with the linear PCA method, the kernel PCA can capture nonlinear functions. In this case, the Z_2 chiral order of the classical spins in these lattices is indeed a nonlinear function of the input spin configurations. In addition to the principal component revealed by the linear PCA, the kernel PCA can find two more principal components using the data generated by Monte Carlo simulation for various temperatures as the input. One of them is related to the strength of the $U(1)$ order parameter, and the other directly manifests the chiral order parameter that characterizes the Z_2 symmetry breaking. For a temperature-resolved study, the temperature dependence of the principal eigenvalue associated with the Z_2 symmetry breaking clearly shows second-order phase transition behavior.

Keywords machine learning, classical XY model, kernel PCA, frustrated lattice

PACS numbers 05.70.Fh

Frontiers of Physics

1 Introduction

Recently, there has been increasing interest in the application of machine learning to the classification of phases of matter [1–18], including both quantum and classical phases with different order parameters [1–15] as well as topological phases [16–18]. The schemes involved include both supervised learning [3, 4, 7, 11–13, 16–18] and unsupervised learning [1, 2, 5, 6, 8–10, 14, 15]. For example, previous works have applied unsupervised learning techniques such as a principal component analysis (PCA) to analyze the data generalized by classical Monte Carlo simulation for both Ising and XY models at different temperatures [1, 2, 8], and they have shown that the PCA method can clearly distinguish between a high-temperature disordered phase and the low-temperature ordered phase.

In the first paper of this series [1], we have applied the PCA method to frustrated classical spin models [19–25] such as the XY model for triangular and Union Jack lattices [26, 27]. Unlike the XY model for the square lattice [28–30], the low-temperature phase in these frustrated models displays both $U(1)$ and Z_2 order parameters, and as the temperature increases, two phase transitions occur, across which the $U(1)$ and Z_2 order parameters disappear separately. For instance, for the Union Jack lattice, the low-temperature phase contains both orders, the intermediate phase only has the $U(1)$ order, the Z_2 order vanishes, and the high-temperature phase has no order. We show that the PCA method applied to the data generated at all temperatures can clearly distinguish all three phases. By applying a PCA to temperature-resolved data, the principal values as a function of the temperature can also reveal the location and nature of the phase transitions. More importantly, we also design a simple toy model to understand why the PCA method can work in this application of recognizing the phase of matter.

Nevertheless, at the end of this paper, we mention the limitations of the PCA method. One limitation is that it does not allow a direct readout of the order parameter. However, we remark that in some cases, the PCA method does allow a direct readout of the order

*arXiv: 1803.01205.

parameter, and the simplest example is the Ising model. In this case, the input data are a set of spin configurations x_n as $\{s_i, \{i = 1, \ldots, L\}\}$, where s_i is the Ising spin at each site and is equal to either $+1$ or -1. The PCA will find one principle component with the eigenvector $(1/L)\{1, 1, \ldots, 1\}$. The projection of each x_n onto this principle component is simply $(1/L)\sum_i s_i$, and this is nothing but the total magnetization and is the order parameter for the Ising model, which captures the Z_2 symmetry breaking.

Taking this Z_2 symmetry breaking as an example, let us be more concrete about the mathematical description of the symmetry breaking for a general situation. Considering a function $f(x)$ with a spin configuration x as the input and a single number $y = f(x)$ as the output and for a set of data $\{x_n\}$, we consider the probability $P(f(x) = y)$, where x runs over all data within the data set. $P(y)$ is also known as the histogram. If $\{x_n\}$ is a high-temperature data set, $P(y)$ will behave as in Fig. 1, which is a symmetric function peaked at $y = 0$; however, for a low-temperature data set $\{x_n\}$, $P(y)$ should be a double-peak symmetric function, as shown in Fig. 1. In the case of the Ising model, $f(x)$ can be simply chosen as the average total magnetization $(1/L)\sum_i s_i$.

However, in the case of the triangular and Union Jack lattices, the Z_2 degree of freedom is the chirality order, which describes the clockwise or anticlockwise spin rotation around each triangle. The PCA method can distinguish phases with different chirality, but it fails to directly characterize the Z_2 symmetry breaking, as mentioned above, simply because the chirality order of this case is a nonlinear function of the input. Consequently, f should also be a nonlinear function.

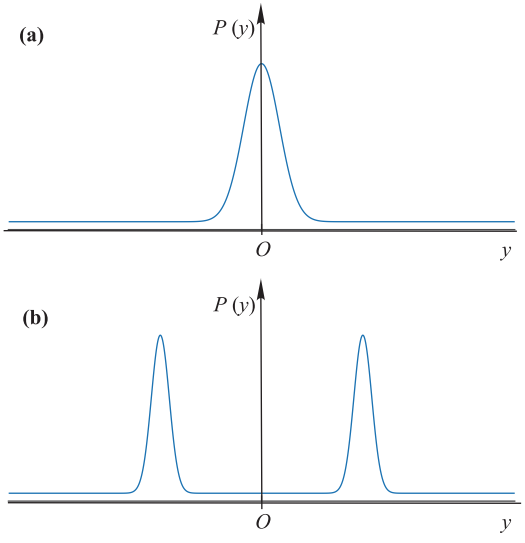

Fig. 1 Schematic of mathematical description of Z_2 symmetry breaking: Histogram $P(y)$ for **(a)** high temperature data set without a Z_2 symmetry breaking and **(b)** low temperature data with a Z_2 symmetry breaking.

In machine learning, a so-called kernel trick is often used to capture the nonlinear characteristics of the order parameter. In this paper, we will apply the kernel PCA method to the XY model for different lattices, and we will show that the kernel PCA method can capture the strength of the $U(1)$ order and allow a direct readout of the Z_2 chirality order. We also design a similar toy model to understand how the kernel PCA method works here.

2 Model and method

Here, we will first briefly review the model we consider and the kernel PCA method [31]. The Hamiltonian of the classical XY model is given by

$$\mathcal{H} = J \sum_{\langle ij \rangle} \boldsymbol{s}_i \cdot \boldsymbol{s}_j, \tag{1}$$

where $\boldsymbol{s}_i = (\cos\theta_i, \sin\theta_i)$ is a classical planar spin defined at each site and $\theta_i \in (0, 2\pi]$, $\langle ij \rangle$ denotes all the nearest-neighbor bonds. Since they are classical models, the data we use are generated by classical Monte Carlo simulation. Such an algorithm can produce equilibrium spin configurations at different temperatures, denoted by $\{x_n\}$ $(n = 1, \ldots, N)$. Each x_n is a vector with a dimension of $2L$, organized as

$$x_n = (\cos\theta_1, \ldots, \cos\theta_L, \sin\theta_1, \ldots, \sin\theta_L), \tag{2}$$

where L is the total number of lattice sites and N is the total number of data points in the data set. $\{x_n\}$ $(n = 1, \ldots, N)$ will be the data and the only input that we feed to a computer. In our analysis below, we will use the data generated at different temperatures as the input in most cases. In some cases specified as a temperature-resolved analysis, we use data with a given temperature as the input.

The kernel PCA method first maps the original data x with a dimension of $2L$ to M-dimensional data $\phi(x)$ with $M > 2L$ by a mapping $\phi(x)$. The PCA for this new data set $\{\phi(x_n)\}$ is called the kernel PCA. We define $\bar{\phi} = (1/N)\sum_{n=1}^{N} \phi(x_n)$ as the average of all data and organize all data into a $N \times M$-dimensional matrix $\mathcal{X}$, where $\mathcal{X}_{nm}$ denotes the m-th component of $\phi(x_n) - \bar{\phi}$. Now, we define an $N \times N$-dimensional matrix $\mathcal{K} = \mathcal{X}\mathcal{X}^T$. It is easy to show that the matrix $\mathcal{K}$ has the same set of eigenvalues as an $M \times M$-dimensional matrix $\mathcal{S} = \mathcal{X}^T\mathcal{X}$. The linear PCA used in the previous paper can be viewed as a special case, where we diagonalize the matrix $\mathcal{S}$ with $\phi(x) = x$. It is straightforward to show that

$$\mathcal{K} = K - \frac{1}{N}E_{N,N}K - \frac{1}{N}KE_{N,N} + \frac{1}{N^2}E_{N,N}KE_{N,N}, \tag{3}$$

where $E_{a,b}$ is an $a \times b$ matrix whose elements are all set to unity and $K_{ij} = \phi(x_i)\phi(x_j)^T$ is denoted by $k(x_i, x_j)$. Here, $k(x, y)$ is called the kernel function. In practice, instead of designing the mapping function $\phi(x)$, we usually directly design the kernel function $k(x, y)$, and it can be proved that each choice of $k(x, y)$ corresponds to a choice of $\phi(x)$.

Since the matrices $\mathcal{K}$ and $\mathcal{S}$ have the same set of eigenvalues, for instance, for the same eigenvalue λ, the corresponding eigenvector for the matrix $\mathcal{K}$ is denoted by $\boldsymbol{v}$ and the corresponding eigenvector for the matrix $\mathcal{S}$ is denoted by $\boldsymbol{u}$, it can be shown that $\boldsymbol{u}$ and $\boldsymbol{v}$ are related by

$$\boldsymbol{u} = \frac{1}{(\lambda)^{1/2}} \mathcal{X}^T \boldsymbol{v}. \tag{4}$$

Suppose that $\boldsymbol{v}_i$ is the eigenvector of $\mathcal{K}$ corresponding to the ith largest eigenvalue. Following Eq. (4), the projection of the general data $\phi(x) - \bar{\phi}$ onto $\boldsymbol{v}_i$ is

$$\mathcal{P}_i(x) = \frac{1}{(\lambda_i)^{1/2}} \sum_{k=1}^{N} v_{ik}[\phi(x) - \bar{\phi}][\phi(x_k) - \bar{\phi}]^T, \tag{5}$$

where v_{ik} is the kth component of $\boldsymbol{v}_i$. A consequence of Eq. (5) is that

$$\mathcal{P}_i(x_j) \propto v_{ij}. \tag{6}$$

Below, we will apply this kernel PCA algorithm with the quadratic kernel $k(x, y) = (xy^T)^2$ to the XY model for several different lattices.

3 Square lattice model

We first apply this method to the square lattice. The input data are generated at temperature ranging from well above the transition temperature to well below the transition temperature. The results obtained using a quadratic kernel are shown in Fig. 2(a), in which we find three eigenvalues that are much larger than all of the rest. Their corresponding eigenvalues are denoted by $\boldsymbol{v}_1$–$\boldsymbol{v}_3$, and the projection of the data x_n into the subspace spanned by these three vectors forms a three-dimensional vector $l_n = \{\mathcal{P}_1(x_n), \mathcal{P}_2(x_n), \mathcal{P}_3(x_n)\}$. These vectors are shown in Fig. 2(b), and they look like a cone.

In the previous work, we have developed a toy model to understand the outcome of the linear PCA. The toy model assumes that $p\%$ of the data are completely ordered; that is, all of the spins at different sites point in the direction θ. The other $(1-p)\%$ of the data are completely disordered, that is, the spins between any two sites are not correlated at all. Here, we show that the same toy model can also be used to understand the meaning of this outcome from the kernel PCA.

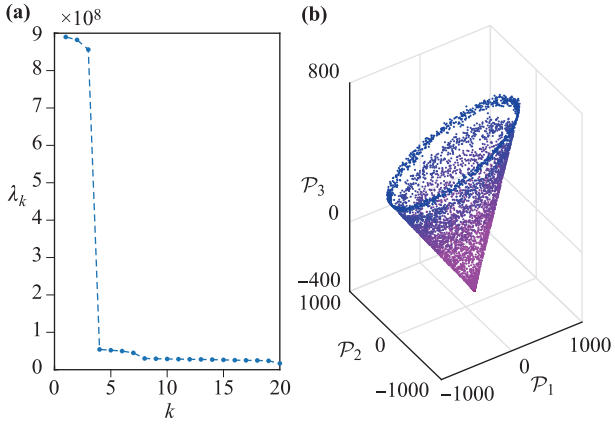

Fig. 2 **(a)** Eigenvalues of the kernel PCA applied to the XY model on $L = 36 \times 36$ square lattice. The temperature of the data set ranges from $0.2J$ to $1.8J$, with $\Delta T = 0.2J$. At each temperature, 1000 samples are collected. There are three eigenvalues much larger than the others. **(b)** The projection of the data into the subspace spanned by the first three largest eigenvectors. The blue data points are low-temperature data and the purple data points are high-temperature data.

With this simplification of the input data, it is easy to show that the $\mathcal{K}$ matrix can be constructed as

$$\mathcal{K} = \begin{pmatrix} K^{\text{low}} + c_1 E_{pN,pN} & c_2 E_{pN,(1-p)N} \\ c_2 E_{(1-p)N,pN} & K^{\text{high}} + c_3 E_{(1-p)N,(1-p)N} \end{pmatrix}, \tag{7}$$

where

$$K^{\text{low}}_{ij} = \frac{L^2}{2}\left[1 + \cos\left(\frac{4\pi(i-j)}{pN}\right)\right], \tag{8}$$

$$K^{\text{high}}_{ij} = L^2 \delta_{ij}, \tag{9}$$

$c_1 = L^2(p^2 - 2p)/2$, $c_2 = -L^2 p(1-p)/2$, and $c_3 = L^2 p^2/2$. Similarly, the eigenvectors corresponding to the largest two eigenvalues of $\mathcal{K}$ are of the form

$$\boldsymbol{v}_1 \propto \left(\cos\left(\frac{4\pi}{pN}\right), \ldots, \cos\left(\frac{4\pi n}{pN}\right), \ldots, \cos(4\pi), 0, \ldots, 0\right), \tag{10}$$

$$\boldsymbol{v}_2 \propto \left(\sin\left(\frac{4\pi}{pN}\right), \ldots, \sin\left(\frac{4\pi n}{pN}\right), \ldots, \sin(4\pi), 0, \ldots, 0\right). \tag{11}$$

It can be shown that the corresponding projections onto $\boldsymbol{v}_1$ and $\boldsymbol{v}_2$ are

$$\mathcal{P}_1(x) \propto \sum_{n,m=1}^{L} \cos(\theta_m + \theta_n), \tag{12}$$

$$\mathcal{P}_2(x) \propto \sum_{n,m=1}^{L} \sin(\theta_m + \theta_n). \tag{13}$$

For fully correlated data, because $\theta_n = \theta_m = \theta$, $\{\mathcal{P}_1(x), \mathcal{P}_2(x)\} \propto \{\cos(2\theta), \sin(2\theta)\}$, which forms a circle. For fully uncorrelated data, averaging over all sites gives rise to vanishingly small numbers. This part contains the information of the $U(1)$ order parameter, and it is nearly the same as the projection onto the first two principal components in the linear PCA case.

Now, we come to the projection onto $\boldsymbol{v}_3$. It can be shown that, within this toy model,

$$\boldsymbol{v}_3 \propto (1-p, 1-p, \ldots, 1-p, -p, -p, \ldots, -p). \tag{14}$$

Therefore,

$$\mathcal{P}_3(x) \propto \sum_{n,m=1}^{L} \cos(\theta_n - \theta_m) + \mathcal{C}, \tag{15}$$

where $\mathcal{C}$ is a constant. It is straightforward to show that

$$\mathcal{P}_1(x) = \mathcal{A}^2 - \mathcal{B}^2, \tag{16}$$

$$\mathcal{P}_2(x) = 2\mathcal{A}\mathcal{B}, \tag{17}$$

$$\mathcal{P}_3(x) = \mathcal{A}^2 + \mathcal{B}^2 + \mathcal{C}, \tag{18}$$

where $\mathcal{A} \propto \sum_{m=1}^{L} \cos(\theta_m)$ and $\mathcal{B} \propto \sum_{m=1}^{L} \sin(\theta_m)$. Thus, one reaches the relation

$$\mathcal{P}_1^2(x) + \mathcal{P}_2^2(x) = \mathcal{P}_3^2(x) + \mathcal{C}. \tag{19}$$

It results in a cone, and this explains the projections shown in Fig. 2(b).

This relation also shows that $\mathcal{P}_3$ has a clear physical meaning; that is, up to a constant, it gives rise to the strength of the $U(1)$ order parameter. Since the PCA is designed to capture the largest variance in the data set, the appearance of this third eigenvalue is therefore due to the fact that the data are generated at different temperatures and the strength of the $U(1)$ order varies between different temperatures. In other words, for a temperature-resolved kernel PCA in which all data are generated at the same temperature, there is nearly no variation in the $U(1)$ order parameter; therefore, this eigenvalue is no longer significantly larger than the others, and there will be only two prominent components, as in the linear PCA case.

4 Triangular lattice

Now, we move to the XY model with antiferromagnetic coupling $J > 0$ on a triangular lattice. For this lattice, at the temperature $T_{c1} = 0.504J$ [26, 27], a Kosterlitz–Thouless transition takes place, below which there exists an algebraic $U(1)$ spin order. Below another transition temperature $T_{c2} = 0.512J$ [26, 27], a discrete Z_2 chiral order forms, and the planar spins around each triangle rotate either clockwise or anticlockwise. For the triangular lattice, since these two transitions are very close, we do not have enough data between these two transition points, and they are regarded as a single transition in practice.

We apply the kernel PCA with the same quadratic kernel to the data of this model generated at nine different temperatures ranging from $0.3J$ to $0.7J$ with $\Delta T = 0.05J$. As shown in Fig. 3, we find that there are a total of six eigenvalues that are significantly larger than the others, among which four (labeled $\lambda_2, \ldots, \lambda_5$) are nearly degenerate. The projections of all data $\{x_n\}$ into the subspace spanned by these four eigenvector are shown in Fig. 4. It looks nearly the same as Fig. 6 of our previous papers, which show the projections of the data into the subspace spanned by all four significantly large eigenvectors found by the linear PCA. In fact, these four eigenvectors have more or less the same meaning as that found by linear PCA. We will not repeatedly discuss them here.

Here, we will mainly focus on the largest eigenvalue and its corresponding eigenvector. As we show in Fig. 5, for high-temperature data, $\mathcal{P}_1$ is mainly concentrated at zero, and for low-temperature data, it exhibits a symmetric double-peak structure. According to what we stated for Fig. 1 in Section 1, it serves the purpose of directly characterizing the Z_2 symmetry breaking.

This principal component can also be understood by a similar "toy model". In this simple "toy model", let us only consider three sites (labeled A, B, and C) in one unit cell. We assume that p% of the data are ordered, among which half have a clockwise chirality order and the other half have an anticlockwise chirality order, and the rest $(1-p)$% of the data are completely disordered. In this case, it is straightforward to show that $\mathcal{K}$ has the same structure as Eq. (7). Because the inner product between data with different chiral orders is zero, K^{low} takes the

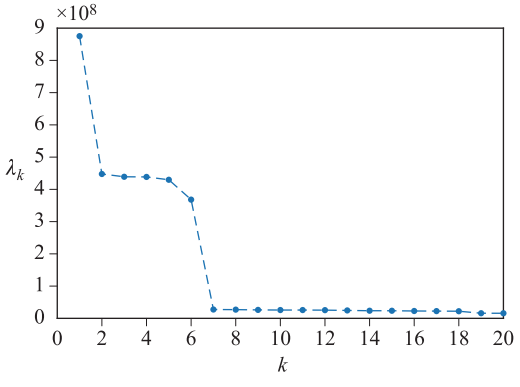

Fig. 3 The eigenvalues of kernel PCA for XY model on $L = 36 \times 36$ triangular lattice. The temperature of the data set ranges from $0.3J$ to $0.7J$, with $\Delta T = 0.05J$. At each temperature, 1000 samples are collected.

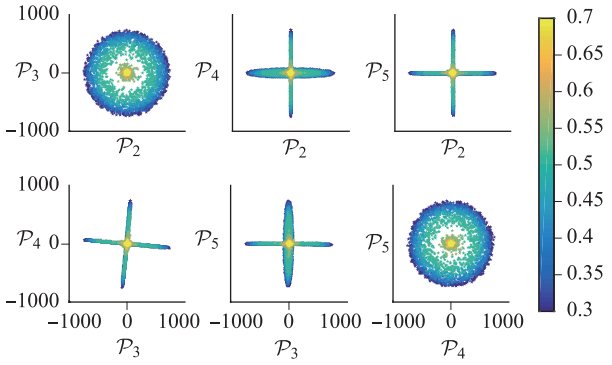

Fig. 4 The projections of kernel PCA onto the 2nd, 3rd, 4th and 5th components for XY model on triangular lattice. The temperature of the data set ranges from $0.3J$ to $0.7J$, with $\Delta T = 0.05J$. At each temperature, 1000 samples are collected.

form of

$$K^{low} = \begin{pmatrix} K^{\uparrow} & 0 \\ 0 & K^{\downarrow} \end{pmatrix}, \tag{20}$$

where

$$K^{\uparrow}_{ij} = K^{\downarrow}_{ij} = \frac{L^2}{2}\left[1 + \cos\left(\frac{8\pi(i-j)}{pN}\right)\right] \tag{21}$$

and $L = 3$. Hence, it is straightforward to show that the largest eigenvector is

$$\boldsymbol{v}_1 = (1, 1, \ldots, 1, -1, -1, \ldots, -1, 0, 0, \ldots 0), \tag{22}$$

where ± 1 correspond to the ordered data with different chirality orders and 0 is for the disordered data. According to Eq. (5), the projection of each datum onto this principal component is

$$\begin{aligned}\mathcal{P}_1(x) \propto \sum_{\theta} \Big\{ \Big[\cos\left(\theta_A - \theta - \frac{2\pi}{3}\right) + \cos\left(\theta_B - \theta + \frac{2\pi}{3}\right) \\ + \cos\left(\theta_C - \theta\right) \Big]^2 - \Big[\cos\left(\theta_A - \theta + \frac{2\pi}{3}\right) \\ + \cos\left(\theta_B - \theta - \frac{2\pi}{3}\right) + \cos\left(\theta_C - \theta\right) \Big]^2 \Big\} \\ \propto \sin(\theta_A - \theta_B) + \sin(\theta_B - \theta_C) + \sin(\theta_C - \theta_A),\end{aligned} \tag{23}$$

which is exactly the chiral order proposed for the triangular-lattice XY model [26, 27].

Here, the sixth eigenvalue for the triangular-lattice XY model is similar to the third eigenvalue for the square-lattice XY model, which represents the strength of the $U(1)$ order parameter. In Fig. 5, we show the projection of all data into the subspace spanned by the first and sixth eigenvectors. Because the $U(1)$ and Z_2 transitions are nearly coincident with each other in this model, Fig. 5 clearly shows that, for data with $\mathcal{P}_1 \approx 0$, the $U(1)$ strength takes the minimum value. When the $U(1)$ strength characterized by $\mathcal{P}_6$ increases toward the maximum, $\mathcal{P}_1$ also shows a feature of Z_2 symmetry breaking.

We also consider a temperature-resolved kernel PCA and focus on the largest eigenvalue associated with this Z_2 chiral symmetry. At each given temperature, we consider several systems with different sizes; then, we perform finite size scaling of this eigenvalue to the infinite size limit. We then plot the eigenvalue at the infinite size limit versus the temperature. The results are shown in Fig. 6, which very clearly displays second-order phase transition behavior. This is consistent with what one expects because this Z_2 transition falls into the Ising universality class and is characterized by a typical second-order Landau transition.

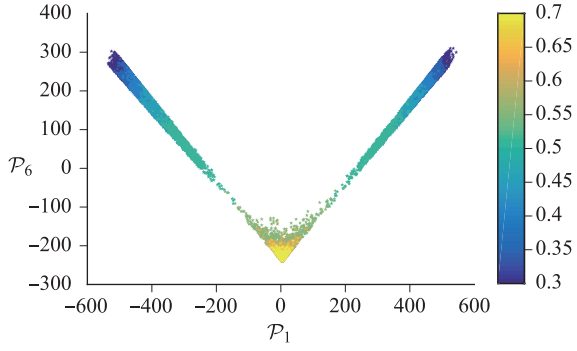

Fig. 5 The projections of kernel PCA onto 1st and 6th components for XY model on triangular lattice. The temperature of the data set ranges from $0.3J$ to $0.7J$, with $\Delta T = 0.05J$. At each temperature, 1000 samples are collected.

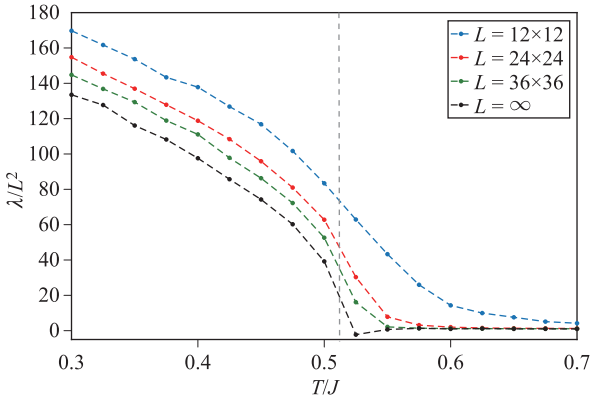

Fig. 6 The largest eigenvalue for temperature resolved kernel PCA. The temperature of the data set ranges from $0.3J$ to $0.7J$, with $\Delta T = 0.025J$. At each temperature, 1000 samples are collected. We perform a finite size scaling to get the result for $L = \infty$.

5 Discussion

We can also apply the same kernel PCA scheme to the Union Jack lattice. The results are quite similar to those for the triangular lattice, and we will not repeat them here. In both cases, we find two more principal components, one of which directly reveals the Z_2 symmetry breaking and the other is associated with the strength of the $U(1)$ order parameter. We could also apply this method to the temperature-resolved case, and the principal component associated with the Z_2 symmetry breaking exhibits the clear signature of a second-order phase transition. Thus, we have satisfactorily addressed the Z_2 order and Z_2 phase transition in these frustrated classical spin models.

However, a common problem for both the nonfrustrated and frustrated classical spin models in two dimensions still remains. Specifically, the $U(1)$ transition is a Kosterlitz–Thouless phase transition and can hardly be captured by these unsupervised learning methods. The reason is because the Kosterlitz–Thouless transition is described by vortex deconfinement and is characterized by a jump in the superfluid density [28–30]. Both vortex deconfinement and the superfluid-density jump are related to the reorganization of the vortex, which is a nonlocal topological object. Progress has been made if the vorticity or velocity fields are used as the input [8, 14, 15], but so far the superfluid-density jump has not been found by machine learning methods using the local spin configuration as the input. On the other hand, a related development has been made in learning topological invariants using neural networks, where the winding number can be accurately predicted using the local Hamiltonian as the input [18]. Therefore, it is conceivable that, by using a supervised learning method to train a neural network, one can capture the Kosterlitz–Thouless transition. We leave this for future studies.

Acknowledgements This work was supported by MOST under Grant Nos. 2016YFA0301600 and NSFC unber Grant No. 11734010.

References

1. C. Wang and H. Zhai, Machine learning of frustrated classical spin models (I): Principal component analysis, *Phys. Rev. B* 96(14), 144432 (2017)
2. L. Wang, Discovering phase transitions with unsupervised learning, *Phys. Rev. B* 94(19), 195105 (2016)
3. J. Carrasquilla and R. G. Melko, Machine learning phases of matter, *Nat. Phys.* 13(5), 431 (2017)
4. E. P. L. van Nieuwenburg, Y. H. Liu, and S. D. Huber, Learning phase transitions by confusion, *Nat. Phys.* 13(5), 435 (2017)
5. G. Torlai and R. G. Melko, Learning thermodyamics with Boltzmann machines, *Phys. Rev. B* 94(16), 165134 (2016)
6. S. Wetzel, Unsupervised learning of phase transitions: From principal component analysis to variational autoencoders, *Phys. Rev. E* 96(2), 022140 (2017)
7. P. Ponte and R. G. Melko, Kernel methods for interpretable machine learning of order parameters, *Phys. Rev. B* 96(20), 205146 (2017)
8. W. J. Hu, R. Singh, and R. Scalettar, Discovering phases, phase transitions, and crossovers through unsupervised machine learning: A critical examination, *Phys. Rev. E* 95(6), 062122 (2017)
9. K. Ch'ng, N. Vazquez, and E. Khatami, Unsupervised machine learning account of magnetic transitions in the Hubbard model, *Phys. Rev. E* 97(1), 013306 (2018)
10. N. C. Costa, W. J. Hu, Z. J. Bai, R. Scalettar, and R. Singh, Principal component analysis for fermionic critical points, *Phys. Rev. B* 96(19), 195138 (2017)
11. S. Wetzel and M. Scherzer, Machine learning of explicit order parameters: From the Ising model to $SU(2)$ lattice gauge theory, *Phys. Rev. B* 96(18), 184410 (2017)
12. K. Ch'ng, J. Carrasquilla, R. G. Melko, and E. Khatami, Machine learning phases of strongly correlated fermions, *Phys. Rev. X* 7(3), 031038 (2017)
13. P. Broecker, J. Carrasquilla, R. G. Melko, and S. Trebst, Machine learning quantum phases of matter beyond the fermion sign problem, *Sci. Rep.* 7(1), 8823 (2017)
14. P. Broecker, F. F. Assaad, and S. Trebst, Quantum phase recognition via unsupervised machine learning, arXiv: 1707.00663 (2017)
15. M. Beach, A. Golubeva, and R. G. Melko, Machine learning vortices at the Kosterlitz–Thouless transition, *Phys. Rev. B* 97(4), 045207 (2018)
16. Y. Zhang and E. Kim, Quantum loop topography for machine learning, *Phys. Rev. Lett.* 118(21), 216401 (2017)
17. Y. Zhang, R. G. Melko, and E. Kim, Machine learning Z_2 quantum spin liquids with quasiparticle statistics, *Phys. Rev. B* 96(24), 245119 (2017)
18. P. Zhang, H. Shen, and H. Zhai, Machine learning topological invariants with neural networks, *Phys. Rev. Lett.* 120(6), 066401 (2018)
19. J. Villain, Spin glass with non-random interactions, *J. Phys. Chem.* 10, 1717 (1977)
20. J. Villain, Two-level systems in spin-glass model (I): General formalism and two-dimensional model, *J. Phys. Chem.* 10, 4793 (1977)
21. D. H. Lee, J. D. Joannopoulos, J. W. Negele, and D. P. Landau, Discrete-symmetry breaking and novel critical phenomena in an antiferromagnetic planar (XY) model in two dimensions, *Phys. Rev. Lett.* 52(6), 433 (1984)

22. S. Miyashita and H. Shiba, Nature of phase transition of the two-dimensional antiferromagnetic plane rotator model on the triangular lattice, *J. Phys. Soc. Jpn.* 53(3), 1145 (1984)

23. S. Lee and K. C. Lee, Phase transitions in the fully frustrated XY model studied with use of the microcanonical Monte Carlo technique, *Phys. Rev. B* 49(21), 15184 (1994)

24. S. Korshunov, Kink pairs unbinding on domain walls and the sequence of phase transitions in fully frustrated XY models, *Phys. Rev. Lett.* 88(16), 167007 (2002)

25. M. Hasenbusch, A. Pelissetto, and E. Vicari, Transitions and crossover phenomena in fully frustrated XY systems, *Phys. Rev. B* 72(18), 184502 (2005)

26. T. Obuchi and H. Kawamura, Spin and chiral orderings of the antiferromagnetic XY model on the triangular lattice and their critical properties, *J. Phys. Soc. Jpn.* 81(5), 054003 (2012)

27. J. P. Lv, T. M. Garoni, and Y. J. Deng, Phase transitions in XY antiferromagnets on plane triangulations, *Phys. Rev. B* 87(2), 024108 (2013)

28. P. Olsson, Monte Carlo analysis of the two-dimensional XY model (II): Comparison with the Kosterlitz renormalization-group equations, *Phys. Rev. B* 52(6), 4526 (1995)

29. T. Ohta and D. Jasnow, XY model and the superfluid density in two dimensions, *Phys. Rev. B* 20(1), 139 (1979)

30. H. Weber and P. Minnhagen, Monte Carlo determination of the critical temperature for the two-dimensional XY model, *Phys. Rev. B* 37(10), 5986 (1988)

31. C. M. Bishop, Pattern Recognition and Machine Learning, Springer, 2007